Journal of Power Sources 195 (2010) 1964–1970

Contents lists available at ScienceDirect

Journal of Power Sources

journal homepage: www.elsevier.com/locate/jpowsour

Autothermal hydrogen generation from methanol in a ceramic microchannel network

Angela M. Moreno, Benjamin A. Wilhite*

Department of Chemical, Materials and Biomolecular Engineering, and Connecticut Global Fuel Cell Center, University of Connecticut, 191 Auditorium Road, Unit 3222, Storrs, CT 06269-3222, USA

ARTICLE INFO

Article history:
Received 28 August 2009
Received in revised form 19 October 2009
Accepted 20 October 2009
Available online 30 October 2009

Keywords:
Cordierite
Microreactors
Combustion
Steam reforming
Process intensification

ABSTRACT

In this paper, the authors present the first demonstration of a new class of integrated ceramic microchannel reactors for all-in-one reforming of hydrocarbon fuels. The reactor concept employs precision-machined metal distributors capable of realizing complex flow distribution patterns with extruded ceramic microchannel networks for cost-effective thermal integration of multiple chemical processes. The presently reported reactor is comprised of five methanol steam reforming channels packed with $CuO/\gamma\text{-}Al_2O_3$, interspersed with four methanol combustion channels washcoated with $Pt/\gamma\text{-}Al_2O_3$, for autothermal hydrogen production (i.e., without external heating). Results demonstrate the capability of this new device for integrating combustion and steam reforming of methanol for autothermal production of hydrogen, owing to the axially self-insulating nature of distributor-packaged ceramic microchannels. In the absence of any external insulation, stable reforming of methanol to hydrogen at conversions >90% and hydrogen yields >70% was achieved at a maximum reactor temperature of 400 °C, while simultaneously maintaining a packaging temperature <50 °C.

1. Introduction

The conversion of hydrocarbon fuels to hydrogen requires a multi-stage network of multiple unique physical (e.g. vaporization) and/or chemical (e.g. steam reforming, partial oxidation) processes [1–3]. The additional constraints of high thermal efficiencies and system portability for power applications (e.g. portable power, on-board propulsion) requires further physical (e.g. heat recovery) and chemical (e.g. combustion) processes to achieve autothermal operation at economical efficiencies [4–7]. In the catalytic production of hydrogen from hydrocarbons, steam reforming remains preferable over partial oxidation, owing to higher theoretical hydrogen yields on a fuel basis. The endothermic nature of steam reforming in turn necessitates efficient heat supply to the reaction zone, typically by burning a portion of the fuel. In portable power applications, heat coupling of exothermic combustion to endothermic steam reforming is achieved either by autothermal reforming, in which both reactions occur within the same catalytic volume [8–10], or through a heat-exchanger reactor configuration in which each reaction is carried out in a separate catalytic volume [11,12].

Methanol provides a promising liquid fuel for portable power owing to its intrinsic characteristics: it is sulfur-free, stores at high energy density, with a large hydrogen content (12%), is readily available, and is reformed at relatively low temperatures (250–300 °C). Coupling combustion (Eq. (1)) and steam reforming (Eq. (2)) in a heat-exchanger reactor offers several advantages over autothermal reforming, including (i) externally controlled separation of exothermic and endothermic process chemistries, (ii) removal of nitrogen separation requirements from reaction products, enabling the use of air as oxidant in combustion processes, and (iii) allowing independent selection of fuel, catalyst and operating parameters for each separate reaction volume [11,12]. This flexible, multi-volume approach to process intensification in reactor design is especially suited to microchannel reactors.

$$CH_3OH + 1/2(n+2m)O_2 \rightarrow (1-n)CO + 2(1-m)H_2 + nCO_2 + 2mH_2O,$$
$$\Delta H_{rxn} = (91 - 283n - 484m)\,kJ\,mol^{-1} \quad (1)$$

$$CH_3OH + nH_2O \leftrightarrow (1-n)CO + nCO_2 + (2+n)H_2,$$
$$\Delta H = (91 - 41n)\,kJ\,mol^{-1} \quad (2)$$

The use of microreactors for process intensification has been widely investigated owing to order-of-magnitude improvements in mass and heat transfer rates, effectively removing fluid–solid transport limitations [13,14]. Furthermore, microtechnology has enabled creation of portable low weight and volume (high energy density) chemical processors capable of integrating multiple

* Corresponding author. Tel.: +1 860 486 3689; fax: +1 860 486 2959.
E-mail address: bwilhite@engr.uconn.edu (B.A. Wilhite).

0378-7753/$ – see front matter © 2009 Elsevier B.V. All rights reserved.
doi:10.1016/j.jpowsour.2009.10.056

processes within one compact unit [5,6,15–26]. Microchannel networks have been fabricated for coupling catalytic combustion with endothermic reforming processes in silicon, [5,15,18,19], silicon oxide [20], stainless steels [21–23] and cordierite ceramic [24–26] in the absence of mass transfer between process flows. In addition, porous silicon dividing walls have been utilized for coupling methanol reforming with hydrogen separation through palladium-catalyst composite membranes [27] and integration with subsequent combustion of rejected gasses for autothermal operation [28].

Materials selection for microreactor construction is guided by several factors, including flexibility of thermal conductivity, ease of introducing catalytic and/or permselective properties, and cost of manufacture. Recent one-dimensional analysis of several heat-exchanger configurations performed by Moreno et al. [29] illustrated how high thermal conductivity materials (e.g. silicon, stainless steel) may significantly limit thermal efficiencies of high temperature microreactors via rapid thermal equilibration of the solid phase. The resulting "near-isothermal slab" effectively (i) limits hot-spot formation for realizing adiabatic reforming temperatures and/or self-insulating designs, [30,31] (ii) forces all processes to operate at a single, average temperature, which (iii) maintains multiple pathways for heat losses through external surface areas (natural convection) and packaging (conduction).

Washcoating of uniform catalytic films onto polished surfaces (typically encountered with micromachined silicon and metal plates) requires additional materials processing to incorporate adhesion layers [32,33]. Likewise, complex etching and lithography processes are required to impart porosity and/or permselectivity to silicon [34,35] for membrane applications. In contrast, ceramics can be readily fabricated via casting or extrusion to yield a broad range of porosities, while catalytic and/or permselective properties may be imparted using well-established methods developed over the past four decades [36–38]. For example, our research group recently utilized a combination of slurry-coating and electroless plating to introduce hydrogen permselectivity via dense palladium films (~7 μm) into porous cordierite ceramic microchannel networks [39].

Additionally, while reactors assembled from individually micromachined layers enjoy the benefit of "numbering up" to achieve scale-up in capacity without altering the performance of the original unit cell, the cost for scaling-up remains linear—this combined with the relatively high cost of micromachining presents a substantial barrier to the economic feasibility of such systems. Perhaps most importantly, the strategy of stacking individual slabs of rows of microchannels limits the complexity of radial distribution schemes, specifically the distribution geometry as well as the maximum number of unique process flows it comprises [7,40]. In comparison to current micromachining methods, in which both fluid distribution and reaction channels are formed in the same process, extrusion technologies offer a means to fabricate large (10^0–10^4) networks of parallel microscale flow channels from a much broader range of materials, at a fraction of the cost of micromachining—in turn focusing the use of precision machining methods on the construction of highly complex distributors/packaging layers.

In this communication, the authors present the first demonstration of a novel strategy for realizing highly integrated, scalable and cost-effective microchemical systems for portable power, capable of converting logistics fuels to hydrogen. Product hydrogen can be employed by next generation electrochemical systems (fuel cell, electrochemical engine, etc.) at efficiencies significantly greater than conventional combustion engine systems. This strategy combines the advantages of two unique routes to materials processing, (i) precision machining of metals with (ii) ceramics extrusion, to realize a new class of microreactor (Fig. 1) with the following

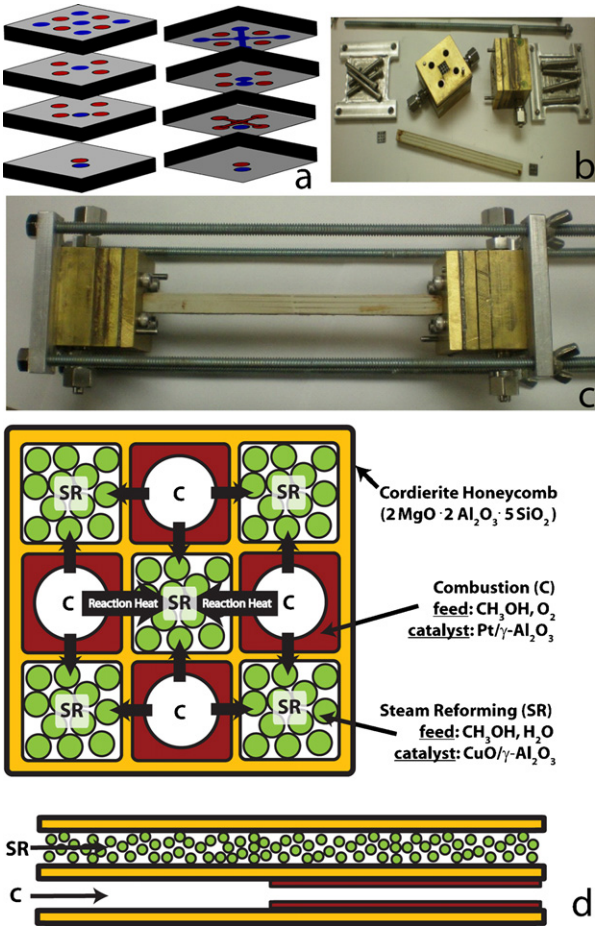

Fig. 1. Distributor-packaged ceramic microchannel network; (a) schematic of distributor assembly from individually machined plates; (b) unassembled portable reactor system showing two distributors, ceramic microchannel network (3 × 3), graphite gaskets and compression chuck; (c) assembled view, and (d) cross-section schematic showing checkerboard distribution and heat transfer vectors.

unique set of advantages: (i) ease of catalyst introduction, via conventional methods (e.g. washcoating), (ii) selectable wall thermal conductivities, via appropriate ceramics selection to enable high temperature operation at a minimum of axial conduction losses, (iii) use of reversible compression fittings for rapid assembly and modification, and (iv) two-dimensional distribution patterns, capable of coupling two or more processes in parallel or series for heat exchange. This fusion of micromachining and extrusion, two unique approaches to materials processing, overcomes existing limitations of microchannel reactors and conventional monoliths to demonstrate a new class of highly integrated chemical reactors. This manuscript details the first implementation of this new reactor concept for autothermal hydrogen production from coupled steam reforming and combustion of methanol.

2. Experimental

The microreactor is comprised of two brass distributors, sealed to either end of the extruded ceramic microchannel network via compression chuck (Fig. 1a and b). Distributors were assembled from individually machined brass plates, and subsequently laminated to form the completed distributor, capable of directly addressing each microchannel with either a combustion (methanol, oxygen) and reforming (methanol, steam) mixture. For the present study, a simple two-fluid checkerboard distribution pattern (Fig. 1d) was employed to demonstrate self-insulating

designs in the axial (1D) dimension. This nine-channel (3 × 3) system represents a basic "unit cell" which may be subsequently scaled up to achieve larger overall capacities without altering the performance of the original cell. The ceramic microchannel network was prepared from a dense, fired cordierite honeycomb monolith, with four channels washcoated with Pt/γ-Al_2O_3 (~200 μm thick) combustion catalyst, and the remaining five channels packed with CuO/γ-Al_2O_3 (−14 + 20 mesh powder) reforming catalyst (Fig. 1c). Distributors were sealed to either end of the microchannel network via reversible compression fittings, using graphite gaskets and a four-point compression chuck (Fig. 1d). Detailed discussion of each step of microreactor construction and testing are presented below.

2.1. Microchannel networks

Ceramic microchannel networks were prepared from 72 cell per square inch (CPSI) dense fired cordierite honeycomb monoliths (Rauschert). Each square channel had a width of 2.5 mm, and the monolith's length was 150 mm. For the present study, 3 × 3 networks were cut from the larger monolith and four individual channels were washcoated with combustion catalyst and five were packed with reforming catalyst, following a checkerboard distribution pattern.

2.2. Catalytic coating (combustion)

Dry catalyst powders were obtained for combustion (1 wt% Pt/Al_2O_3 powder) from Sigma–Aldrich. Catalyst slurry was prepared by mixing catalyst powders with colloidal alumina dispersion (20 wt%, Aldrich) and methanol at a ratio of 11:23:66 by mass, followed by the addition of concentrated Nitric acid solution to initiate gel formation. Slurry was injected into four individual channels in a checkerboard pattern and excess solution removed by pressurized gas. Each channel received eight such coatings of the slurry, allowing for 45 min of drying time at room temperature between coats. Combustion channels were coated such that the first half of the channel length is devoid of catalyst, thus isolating a catalytic "ignition point" at the mid-point of the channel (Fig. 1d). Coated monoliths were then calcined at 450 °C for 4 h (heating rate 2 °C min^{-1} and cooling rate of 2 °C min^{-1}) under an O_2/Ar/He atmosphere. Resulting catalytic coatings of thickness 200–300 μm were verified by scanning electron microscopy (SEM) analysis to be uniform and crack-free (see Fig. 2b).

2.3. Packed minichannels (steam reforming)

After monolith was washcoated with Pt/Al_2O_3, the remaining five channels were packed with copper (II) oxide, 13 wt% on alumina, −14 + 20 mesh (Sigma–Aldrich), corresponding to a particle size of 841–1575 μm. Sample catalyst was loaded on top of a nickel mesh (100 μ) screens that serve as catalyst retainers at either end of individual reforming channels. Approximately 400 mg of catalyst was introduced into each channel. The loading length of the catalyst was about 14 cm. It is critical to fabricate each nickel screen of the same size and weight and place them into each channel at the same depth; this in order to reduce the pressure drop along the reactor and avoid flow maldistribution or gas channeling through the network.

2.4. Distributor construction

Distributors were fabricated from 1/8″ × 2″ × 2″ brass plates. Each plate was machined with three patterns, one on either face of the plate with an intermediate pattern to provide fluidic connections between elements of each face (see Fig. 3). All pattern features were 1/16″, including outlet ports addressing each microchannel.

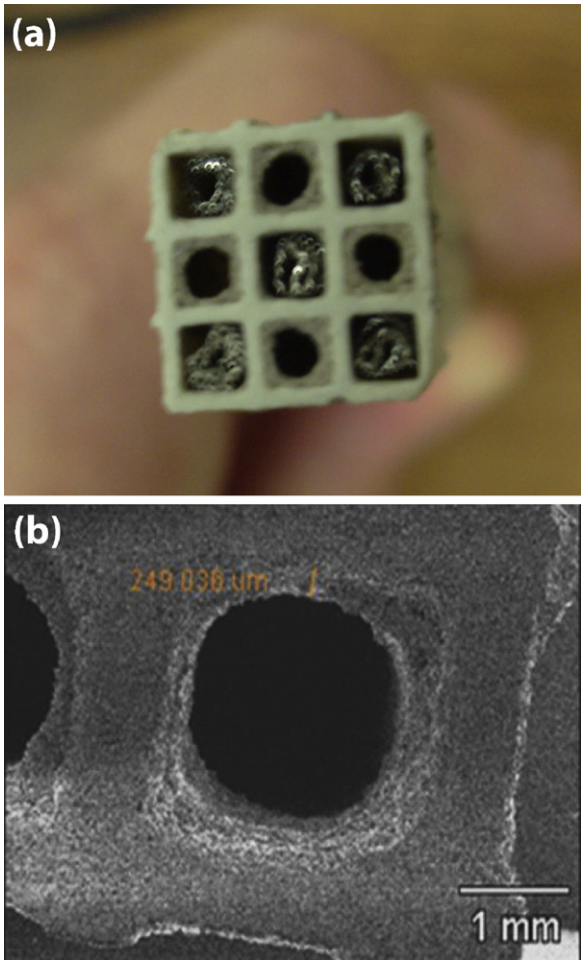

Fig. 2. SEM images of 1 wt% Pt/Al_2O_3 catalyst deposited monolith.

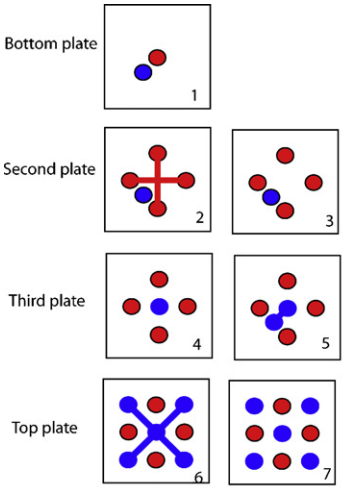

1. Bottom plate: Fluid A and fluid B main inlets
2. Second plate:- Bottom: Fluid A undergoes first level bifurcation
3. Second plate - Top: End of first bifurcation
4. Third plate - Bottom: Second level bifurcation of fluid A, first level bifurcation of fluid B
5. Third plate - Top End of second bifurcation level
6. Top plate - Bottom: Second level bifurcation of fluid B
7. Top plate - Top: End of third bifurcation level

Fig. 3. Schematic of distributor layers for two-fluid process integration in a checkerboard configuration.

The bottom plate was made from a thicker (1″) slab to accommodate standard 1/8″ nominal pipe thread (NPT) fittings. The top-most plate was designed with a 1/16″ deep recess to allow proper seating of a high temperature graphite compression gasket for reversibly sealing the distributor to the ceramic microchannel network. Lamination of the individual layers to form the completed distributor was accomplished using a high temperature gasket between each individual layer. The resulting distributor uniformly distributes separate steam reforming and combustion flows amongst the microchannel network in a checkerboard distribution pattern, to minimize thermal gradients in the radial plane; thus, self-insulating properties of the ceramic microchannel network can be verified in the axial dimension.

2.5. Microreactor assembly

The microchannel network was assembled by compression sealing of distributors to either end of the extruded ceramic microchannel network as follows. Graphite gasket sheets (1/16″, McMaster-Carr) were placed in the recessed face of each distributor, followed by either end of the ceramic network. Compression sealing was accomplished by a four-point compression chuck placed around the assembly and tightened by hand.

2.6. Microreactor operation

The assembled microreactor was investigated for the autothermal production of methanol via thermally coupled methanol combustion and steam reforming. Performance of the microreactor is determined via gas effluent analysis using an Agilent Micro-Gas Chromatograph; thermal images were obtained during steady autothermal operation using an FLIR Thermacam™ infrared camera with an accuracy of ±2 °C. The Thermacam™ was positioned 5 ft away from experiment and it was set up to take the thermal images of the visible surface. Therefore, all reported temperatures correspond to the monolith external surface/wall.

The combustion gas was comprised of a dry gas blend of (i) 19.95% oxygen/4.797% helium/argon diluted with (ii) ultra-high-purity argon and subsequently enriched with methanol vapor to 4.0% using a gas washer/humidifier. In this manner, the amount of oxygen supplied to the combustion channels can be varied while maintaining a constant rate of fuel addition. The reforming gas was comprised of 2.8% methanol/2.8% steam in 5% nitrogen/argon mixture. Methanol and/or water reagents were supplied by passing dry gas mixtures through thermostated bubblers containing 100% purity methanol (J.T. Baker) and a 1.5 (v/v) mixture of distilled water and methanol, for combustion and steam reforming respectively. Both reforming and combustion feeds entered the reactor at ambient temperature (no preheating). Argon was employed as the carrier gas, with helium and nitrogen serving as internal standards for quantifying conversion yield and cross-over in the combustion and reforming channels, respectively. Oxygen content was varied such that the equivalence ratio (ER), defined as the ratio of oxygen to fuel relative to the stoichiometric ratio (Eq. (3)), ranged from 0.5 to 1.0. The total combustion flow rate was fixed at 900 sccm corresponding to a Reynold's number of 450 within each combustion cell and the total reforming flow rate fixed at 300 sccm, corresponding to a Reynold's number of 120 within each reforming cell.

$$\mathrm{ER} = \frac{F_{O_2}}{1.5 \times F_{CH_3OH}} \tag{3}$$

Effluent gas streams were analyzed on a dry basis by gas chromatography; condensable species were removed by a sequence of two condensers maintained at 273 and 195 K. A dual-column Agilent MS3000 gas chromatograph equipped with Molecular Sieve and Plot Q columns and Cerity NDS software was used in all experiments. Both columns were operated at a temperature of 60 °C, and a column head pressure of 30 and 18 psia respectively, with 4 min run-time to effectively separate the species of interest. The gas chromatograph was calibrated using known concentrations of each species (CO, N_2, H_2, CO_2 and CH_4). Gas samples from the reactor were analyzed once the system had reached steady state, approximately 2 h after system start-up. Ten samples were analyzed at each set of conditions studied, with averaged peak areas being used to determine gas composition. The extent of methanol conversion was calculated from the molar flow rates concentration of methane, carbon monoxide and carbon dioxide in the product gas, using the carbon balance (Eq. (4)):

$$X_{CH_3OH} = \frac{F_{CO} + F_{CH_4} + F_{CO_2}}{F_{CH_3OH,\,in}} \tag{4}$$

3. Results

All experiments were performed in the absence of any external heating or insulation, in order to demonstrate the self-insulating properties of the ceramic microchannel network under purely autothermal operation. Combustion flow rate was held constant at a total flow rate 900 sccm, corresponding to a gas hourly space velocity of 90,000 h^{-1} (Eq. (5)) and a Reynold's number of 450 within each cell. Reforming flow rate was held constant at a total flow rate of 300 sccm, corresponding to a gas hourly space velocity of 27,000 h^{-1}, and a composition of 2.8% methanol/2.8% steam and 5% nitrogen internal standard in argon. In this manner, reactor operation is controlled solely through the combustion equivalence ratio. Details of combustion channel performance (hot-spot magnitude, stability, location) and reforming channel performance (hydrogen yield, selectivities) are presented below.

$$\mathrm{GHSV} = \frac{\text{volumetric flow per channel}}{\text{single channel volume}} \tag{5}$$

3.1. Performance of combustion channels

The performance of the combustion channels was first evaluated as a function of equivalence ratio by thermal imaging to identify steady state hot-spot location and magnitude. Hot-spot position is referenced to the center of flame relative to the distributor outlet. The reactor was initially supplied with a stoichiometric O_2/CH_3OH ratio (ER = 1) to achieve autocatalytic ignition (without any external heat addition). Once the system was ignited and the flame stabilized, the fuel composition was reduced from ER = 1–0.6 at intervals of 0.1 while maintaining a constant flow rate of 900 sccm.

During system start-up (ER = 1) a localized hot-spot formed at the ignition point, located mid-way along the reactor axial length where methanol and oxidant mixture first contact the catalytic coating. At this point the flame had a symmetrical and broad shape, with a width of 2 cm and maximum temperature of 450 °C. After ignition, the reaction zone was observed to slowly migrate upstream, finally stabilizing at a position ~1 cm from the distributor outlet. There is no observed change in the maximum hot-spot temperature after flame separation from the ignition point. This separation of a stable hot-spot from the catalytic zone indicates a homogeneous flame forms within the combustion channels.

As ER is reduced, the reaction zone shifts downstream, the flame broadens, and the maximum temperature of the hot-spot decreases (owing to reduced methanol conversion). The temperature of the surface reduces from 450 °C, located near the distributor at an ER of unity, down to 300 °C located near the center of the microchannel network at an ER of 0.6. The hot-spot magnitude and location relative to the reactor inlet as a function of decreasing ER are shown in Fig. 4. At ER = 0.6 the system is still ignited, with an elongated flame stabilized near the middle of the reactor with a hot-spot

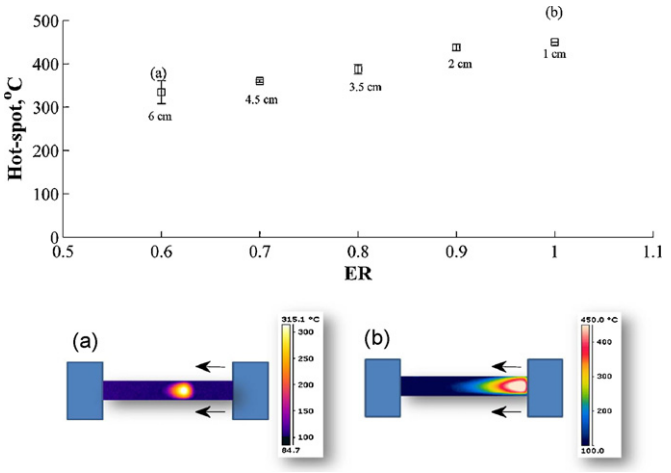

Fig. 4. Hot-spot location relative to reactor inlet, including thermal imaging obtained for (a) hot-spot located at the ignition point, and (b) hot-spot located at the reactor inlet. Thermal images of the microchannel network under steady autothermal operation were obtained via FLIR Thermacam™ infrared camera.

magnitude of about 300 °C. Further reductions in ER resulted in flame extinction, as oxygen supply was insufficient to maintain ignition.

By placing the hot-spot in the center of the reactor, a self-insulating length of ceramic is created between the reaction zone and the distributors for maximum thermal efficiency. Due to the limited axial heat conduction associated with low thermal conductivity (2 W m^{-1} K^{-1}) cordierite, the process is thermally self-sustaining with a minimum temperature increase in the brass distributors (around 40–50 °C), making the device safe and easy to handle. These phenomena had been previously investigated theoretically by Moreno et al. [29], who predicted that low thermal conductivity substrates would enable placement of a hot-spot in the middle of the reactor, in turn achieving high thermal efficiency.

3.2. Performance of steam reforming channels

The effect of O_2/CH_3OH molar ratio on the performance of the microchannel combustor is summarized in Fig. 5a (Solid and empty squares represent results in the steam reforming and combustion channels respectively). As expected, the extent of methanol conversion decreases with equivalency ratio (ER). As the ER was reduced from 1 to 0.6, conversion reduced from 84% to 55%. The decreased conversion at lower ER is consistent with other microscale combustion devices [40] and it is due to limited amount of oxidizer in the feed below its stoichiometric value. The performance of the autothermal reformer as function of combustor ER (and therefore hot-spot magnitude and location) is summarized in Fig. 5b–e. As mentioned previously, a total flow rate of 300 sccm was maintained at a composition of 2.8% methanol/2.8% steam in 5% nitrogen/argon mixture for all experiments, corresponding to a gas hourly space velocity of 27,000 h^{-1}.

The presence of helium in the reforming effluent, verified by gas chromatography, indicates a finite amount of gas cross-over from combustion to reforming channels. This is attributed to a slight porosity within the fired cordierite microchannel network and the overall pressure differential between combustion and reforming channels. Cross-over rates remained constant throughout all experiments and correspond to a less than 4% increase in the total reforming gas flow rate. While it has not been investigated in the present study, the presence of low flow cross-over within channels motivates the integration of membranes for hydrogen separation operations into the microchannel device. This idea has already been explored in our research group by Kim et al. [39], who successfully incorporated palladium permselective membranes into a cordierite microchannel network for hydrogen purification.

Methanol conversion in the steam reforming channels remained constant within experimental error over the span of the combustor equivalence ratio (ER) studied, with greater than 70% methanol conversion achieved for all experiments. Catalyst activity for steam reforming did not noticeably decrease over the course of multiple experiments (10 h on-stream). At high ER values (ER > 0.7) the main

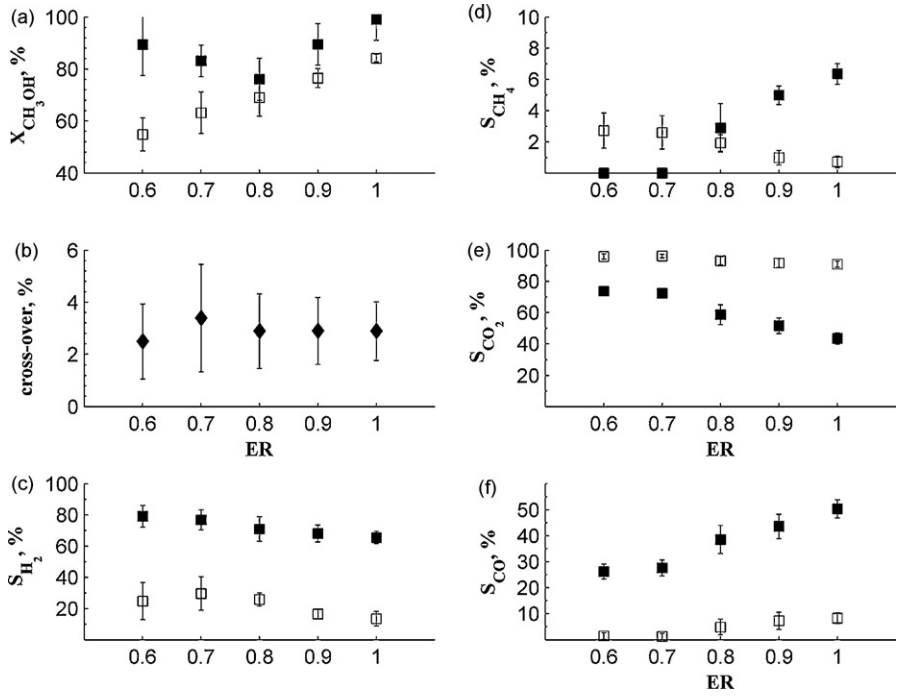

Fig. 5. Effect of equivalence ratio on (a) methanol conversion, (b) cross-over percentage in the reforming side, (c) hydrogen selectivity, (d) methane selectivity, (e) carbon dioxide selectivity, and (f) carbon monoxide selectivity. Steam Reforming (Solid), Combustion (Open).

reaction components are H_2, CO_2, CO and CH_4; methane levels drop below detection limits with further reduction in ER. In addition, since O_2/CH_3OH mixture was fed into the system at stoichiometric ratios less than unity, the combustor effluent also contained hydrogen, in addition to carbon dioxide and unreacted methanol. The influence of combustion ER on selectivity for hydrogen, methane and carbon dioxide is presented in Fig. 5d–f. Selectivity of individual species was calculated according to Eq. (6):

$$S_i = \frac{n_i}{\sum n_i} \times 100 \quad (6)$$

As the operating temperature increases from 330 to 450 °C by increasing ER from 0.6 to 1, $S_{H_2}^{ref}$ and $S_{CO_2}^{ref}$ drop by ~20 and ~30% respectively, while S_{CO}^{ref} increases by ~25%. The drop in hydrogen selectivity can be attributed in part to a change in the water–gas-shift equilibrium to the reactant-side as heat accumulates within the reforming zone (i.e., increasing hot-spot magnitude). These results demonstrate the importance of controlling the hot-spot maximum temperature and location through selection of steady state ER and appropriate start-up procedures. Water-gas-shift reaction produces one mole of H_2 per mole of CO_2; thus the discrepancy in selectivity drop between H_2 and CO_2 suggests additional contributions from other side-reactions, such as methanation or Boudouard reaction; the latter of which may contribute to carbon formation within the reforming channels over the course of experiments. It is important to note that each data point presented herein represents a stable steady state maintained for 2 h without any measurable drop in reactor performance; in this manner, the total time on-stream for the reforming catalyst was approximately 100 h. Upon completion of all experiments, the catalyst was removed from the reforming channels and it was observed to present a color change from dark green to red suggesting some modification of the catalyst surface. While these observations indicate the need for subsequent materials analysis of catalyst to ascertain influence of reforming conditions upon surface structure, this remains the subject of a future study; the focus of the present report is to demonstrate the validity of the ceramic microchannel network concept for autothermal reforming.

CO_2 is the main component produced in the combustion channels for the entire ER range studied. As stated above, some H_2, CO and CH_4 are also produced due to sub-unity equivalency ratios. Pt/Al_2O_3 catalyst shows high selectivity (>95%) towards CO_2 and it remains constant throughout the experiments; however, as ER increases, both $S_{H_2}^{comb}$ and $S_{CH_4}^{comb}$ decrease.

4. Discussion

In this study, the best operating conditions for the autothermal reforming of methanol corresponded to a combustion composition of 10% oxygen/9.1% methanol in helium/argon (ER = 0.6) at a per-channel Reynold's number of 450. The reformer side was supplied at a total flow rate of 300 sccm (GHSV of 27,000 h^{-1}) at a composition of 2.8% methanol/2.8% steam in 5% nitrogen/argon mixture. At these conditions, 90% conversion of methanol with 70% hydrogen yield is observed for the endothermic steam reforming, corresponding to an overall hydrogen yield of 11% in the complete absence of any external insulation. These results validate this novel approach to microreactor design and construction, while confirming that ceramic microchannel reactors are capable of realizing compact, cost-efficient and axially self-insulating designs with promise for autothermal, all-in-one reformers.

In addition to the above advantages, this approach to microreactor construction enables cost-effective scale-up without modifying either the "unit cell" design or the procedure for assembly. This is achieved in the distributor by "numbering up" or replicating the "unit cell" distribution pattern to achieve the desired overall capacity. This poses a relatively linear increase in distributor cost; however the increase in cost of distributor manufacture is outweighed by the negligible increase in microchannel construction costs with scale-up. Larger microchannel networks may be simply cut from original honeycomb monolith substrates; typical monolith substrates provided by industrial manufacturers are 150 mm × 150 mm or larger (>30 in^2), with cell densities of up to 600 cells per square inch available—thus a single microreactor cartridge may contain in excess of 10^4 individual channels without any modifications to industry-standard monolith manufacturing methods.

Thermal efficiency of the presented system is expected to increase with scale-up, as the ratio of external surface area to internal reactor volume decreases, thus reducing the relative amount of heat losses to ambient. Further improvements in thermal efficiency may be realized by continued development of complex radial distribution patterns.

While the present study demonstrates the value of this approach for realizing self-insulating designs in the axial (flow) dimension, the introduction of an additional outer layer of preheating channels around the 3 × 3 core of reforming/combustion channels is expected to provide self-insulating properties in the radial dimensions. Additionally, based upon the optimal flow rate and equivalency ratio of the combustor channels reported herein, modification of the relative distribution of reforming volume and combustion volume within the microchannel network is expected to further improve overall system performance. Recently, our research group demonstrated the ability to incorporate hydrogen permselective membranes within similar, porous, cordierite microchannel networks [39]. The present report verifies not only the applicability of this approach for realizing thermally integrated microreactors, but also the ability to fabricate compact micromembrane systems. Our research group is actively pursuing the addition of palladium-based hydrogen permselective membranes and an outer shell of sweep channels to the existing autothermal reformer design for high-purity hydrogen production. Lastly, work is currently underway in collaboration with the Cornell Nanofabrication Facility to reduce overall system volume and weight by fabricating distributors out of single crystal silicon using lithography-based deep reactive ion etching methods.

5. Conclusions

In this manuscript, the authors detail a novel approach to the design and manufacture of integrated ceramic microchannel reactors for multi-stage reforming of hydrocarbons to hydrogen for fuel cell systems. Results demonstrate the capability of this new device for integrating combustion and steam reforming of methanol for autothermal production of hydrogen, owing to the axially self-insulating nature of distributor-packaged ceramic microchannels. In the absence of any external insulation, stable reforming of methanol to hydrogen at conversions >90% and hydrogen yields >70% were achieved at a maximum reactor temperature of 400 °C, while simultaneously maintaining a packaging temperature <50 °C (as confirmed by thermal images presented in Fig. 4).

Acknowledgements

The authors gratefully acknowledge Peter Menard of the Connecticut Global Fuel Cell Center for his invaluable technical assistance, and Joseph Csiki and Mark Drobney of the Technical Services Facility for machining of the brass distributors. This research was funded by the Office of Naval Research (Grant No. N000140710828) and the DuPont de Nemours Corporation

(through award of a DuPont Young Professor Grant). Benjamin A. Wilhite gratefully acknowledges a Junior Faculty Summer Fellowship by the University of Connecticut.

References

[1] J.D. Holladay, J. Hu, D.L. King, Y. Wang, Catal. Today 139 (2009) 244–260.
[2] C. Song, Catal. Today 77 (2002) 17–40.
[3] A.F. Ghenciu, Curr. Opin. Solid State Mater. Sci. 6 (2002) 389–402.
[4] J.D. Holladay, Y. Wang, E. Jones, Chem. Rev. 104 (2004) 4767–4790.
[5] K. Shah, R.S. Besser, J. Power Sources 166 (2007) 177–193.
[6] A. Qi, A. Peppley, K. Karan, Fuel Process. Technol. 88 (2007) 3–22.
[7] B.A. Wilhite, in: A. Mitsos, P.I. Barton (Eds.), Microfabricated Power Generation Devices: Design and Technology, Wiley-VCH, New York, 2009 (Chapter 7).
[8] P.J. Dauenhauer, B.J. Dreyer, N.J. Degenstein, L.D. Schmidt, Angew. Chem., Int. Ed. 46 (2007) 5864–5867.
[9] L. Ma, D.L. Trimm, C. Jiang, Appl. Catal. 138 (1996) 275–283.
[10] A. Qi, S. Wang, C. Ni, D. Wu, Int. J. Hydrogen Energy 32 (2007) 981–991.
[11] Z. Anxionnaz, M. Cabassud, C. Gourdon, P. Tochon, Chem. Eng. Proc.: Process Intensifcation 47 (2008) 2029–2050.
[12] R.C. Ramaswamy, P.A. Ramachandran, M.P. Dudukovic, Chem. Eng. Sci. 61 (2006) 459–472.
[13] K.F. Jensen, AIChE J. 45 (1999) 2051–2054.
[14] W Ehrfeld, V. Hessel, H. Lowe, Microreactors: New Technology for Modern Chemistry, Wiley-VCH, New York, 2000.
[15] L.R. Arana, S.B. Schaevitz, A.J. Franz, M.A. Schmidt, K.F. Jensen, J. Microelectromech. Syst. 12 (2003) 600–612.
[16] H. Sahoo, J.G. Kralj, K.F. Jensen, Angew. Chem., Int. Ed. 46 (2007) 5704–5708.
[17] B.A. Wilhite, K.F. Jensen, T.F. Hill, L.F. Velasquez-Garcia, A.H. Epstein, C. Livermore, AIChE J. 54 (2008) 2441–2455.
[18] K. Hwang, A. Kim, J. Power Sources 156 (2006) 253–259.
[19] O.J. Kwon, D.H.O. Yoon, J.J. Kim, Chem. Eng. J. 140 (2008) 466–472.
[20] T. Terazaki, M. Nomura, K. Takeyama, O. Nakamura, T. Yamamoto, J. Power Sources 145 (2005) 691–696.
[21] E.R. Delsman, M.H.J.M. DeCroon, G.J. Kramer, P.D. Cobden, Ch. Hofmann, V. Cominos, J.C. Schouten, Chem. Eng. J. 101 (2004) 123–131.
[22] G.-G. Park, S.-D. Yim, Y.-G. Yoon, W.-Y. Lee, C.-S. Kim, D.-J. Seo, K. Eguchi, J. Power Sources 145 (2005) 702–706.
[23] L. Pan, S. Wang, Int. J. Hydrogen Energy 90 (2005) 973–979.
[24] G. Kolios, J. Frauhammer, G. Eigenberger, Chem. Eng. Sci. 57 (2002) 1505–1510.
[25] J. Frauhammer, G. Eigenberger, L. Hippel, D. Arnt, Chem. Eng. Sci. 54 (1999) 3661–3670.
[26] C. Schmitt, D.W. Agar, F. Platte, S. Buijssen, B. Pawlowski, M. Duisberg, Chem. Eng. Technol. 28 (2005) 337–343.
[27] B.A. Wilhite, S.E. Weiss, J.Y. Ying, M.A. Schmidt, K.F. Jensen, Adv. Mater. 18 (2006) 1701–1704.
[28] K.T. Deshpande, B.A. Wilhite, M.A. Schmidth, K.F. Jensen, AIChE Annual Meeting Conference Proceedings, 2005, pp. 9433–9434.
[29] A. Moreno, K. Murphy, B.A. Wilhite, Ind. Eng. Chem. Res. 47 (2008) 9040–9054.
[30] P.D. Ronney, Combust. Flame 13 (2003) 421–439.
[31] Z.J. Shao, W.C. Mederos, W.C. Chueh, S.M. Haile, J. Power Sources 162 (2006) 589–596.
[32] S.-M. Hwang, O.J. Kwon, J.J. Kim, Appl. Catal. A 316 (2007) 83–89.
[33] S. Srinivas, A. Dhingra, H. Im, E. Gulari, Appl. Catal. A 274 (2004) 285–293.
[34] A.J. Franz, K.F. Jensen, M.A. Schmidt, Proceedings of the IEEE: Microelectromechanical Systems (MEMS), 1999, pp. 382–387.
[35] S.-Y. Ye, S. Tanaka, M. Esashi, S. Hamakawa, T. Hanaoka, F. Mizukami, J. Micromech. Microeng. 25 (2005) 2011–2018.
[36] H.-J. Dietzsh, Apparatus for Manufacturing Ceramic Elements Having a Honeycomb Structure, U.S. Patent 3,406,435, 1968.
[37] S.T. Gulati, Ceramic Catalyst Supports for Gasoline Fuel, Structured Catalysts and Reactors, Marcel Dekker Inc., New York, 1998.
[38] T.A. Nijhuis, A.E.W. Beers, T. Vergunst, I. Hoek, F. Kapteijn, J.A. Moulijn, Catal. Rev. Sci. Eng. 43 (2001) 345–380.
[39] D. Kim, A. Kellogg, E. Livaich, B. Wilhite, J. Membr. Sci. 340 (2009) 109–116.
[40] S. Tanaka, T. Yamada, S. Sugimoto, J.-F. Li, M. Esashi, J. Micromech. Microeng. 13 (2003) 502–508.